TOWARDS A MODEL-INDEPENDENT MEASUREMENT OF THE HALO MASS FUNCTION WITH OBSERVABLES

Fuyu Dong¹, Jun Zhang^{1,2*}, Xiaohu Yang^{1,2,3}, Jiajun Zhang¹, Wentao Luo⁴

¹Department of Astronomy, Shanghai Jiao Tong University, Shanghai 200240, China

²Shanghai Key Laboratory for Particle Physics and Cosmology, Shanghai 200240, China

³Tsung-Dao Lee Institute, Shanghai Jiao Tong University, Shanghai 200240, China

⁴Institute for the Physics and Mathematics of the Universe (Kavli IPMU, WPI), UTIAS,
Tokyo Institutes for Advanced Study, University of Tokyo, Chiba, 277-8583, Japan

Draft version May 29, 2019

ABSTRACT

In the CDM paradigm, the halo mass function is a sensitive probe of the cosmic structure. In observations, halo mass is typically estimated from its relation with other observables. The resulting halo mass function is subject to systematic bias, such as the Eddington bias, due to the scatter or uncertainty in the observable - mass relation. Exact correction for the bias is not easy, as predictions for the observables are typically model-dependent in simulations. In this paper, we point out an interesting feature in the halo mass function of the concordence Λ CDM model: the total halo mass within each evenly-spaced logarithmic mass bin is approximately the same over a large mass range. We show that this property allows us to construct an almost bias-free halo mass function using only an observable (as a halo mass estimator) and stacked weak lensing measurements as long as the scatter between the true halo mass and the observable-inferred mass has a stable form in logarithmic units. The method is not sensitive to the form of the mass-observable relation. We test the idea using cosmological simulations, and show that the method performs very well for realistic observables.

 $Subject\ headings: \ Cosmology:\ halo\ mass\ function\ -\ Statistics:\ Eddington\ bias\ -\ Gravitational\ lensing:\ weak$

1. INTRODUCTION

In the CDM cosmological models, dark matter halos grow hierarchically from small perturbations in the initial density field (Lacey and Cole 1993). The abundance of halos as a function of the halo mass is an important probe for cosmology (Press and Schechter 1974; White et al. 1993). In observations, halo mass can be estimated with certain observables, such as the total luminosities of the member galaxies (Vale and Ostriker 2004), the number of the member galaxies (Sheldon et al. 2009; Bauer et al. 2012; Mandelbaum et al. 2008), the X-ray emission from hot gas (Pratt et al. 2009), the gravitational lensing signals (Bartelmann and Schneider 2001; Schneider 2005), the Sunyaev-Zeldovich effect (Sunyaev and Zeldovich 1972), the galaxy velocity dispersion (Biviano et al. 2006; Munari et al. 2013), etc.. In terms of constraining cosmology, recent efforts have mainly focused on combining the halo abundance with their spatial clustering information (Lima and Hu 2005), preferably with a comprehensive modelling of the observation with a large mock sample (Jing et al. 1998; Berlind and Weinberg 2002; Yang et al. 2003; Zheng et al. 2005; van den Bosch et al. 2007; Zehavi et al. 2011; Leauthaud et al. 2011; Yang et al. 2012; Rodríguez-Puebla et al. 2015; Zu and Mandelbaum 2016; Guo et al. 2016; Rodríguez-Puebla et al. 2017; Guo et al. 2018; Obreschkow et al. 2018).

Nevertheless, a direct and accurate measurement of the halo mass function in observation is still not easy. This is due to several reasons: 1) predictions of most observables in simulations are currently model-dependent; 2) the mass - observable relation typically contains a signif-

icant scatter, causing the so called Eddington bias Eddington (1913); 3) the definition of halo mass in simulation has subtle differences for different types of observables; 4) accuracy of weak lensing mass measurement on individual halos is limited by the number density of background source images and the uncertainties of the foreground halo shapes; 5) the completeness of the halo catalog from observation needs to be known very well to form a reasonable comparison with simulation predictions. For the halo mass function to become a useful probe for precision cosmology, the above problems need to be addressed or avoided, ideally in a modelindependent way. This is our motivation. We propose a solution that has the potential of avoiding most, if not all, of the above problems in the measurement of the halo mass function.

Weak lensing is the most direct way of measuring halo mass. So far, lensing is commonly used for calibrating the mass - observable relation through the modeling approach. By grouping the foreground sources according to a particular observable, e.g., luminosity, stellar mass, etc. (Leauthaud et al. 2017; Simet et al. 2017; Murata et al. 2018), their stacked background shear distribution are used to constrain the model parameters in the mass observable relation. Here, we point out that the lensingreconstructed mean mass of halos binned by sorting a certain observable can sometimes be directly interpreted as an accurate estimation of the halo mass function, albeit in a slightly unconventional form: the halo mass as a function of the mass order/rank within a certain cosmic volume. This forms an almost model-independent way of estimating the halo mass function, as we show in the rest of the paper.

We call the new form of the halo mass function the

^{*}betajzhang@sjtu.edu.cn

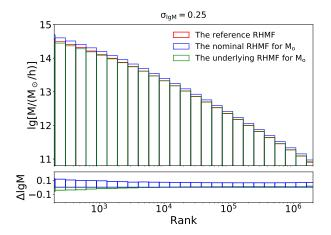


Fig. 1.— Results for the Ranked Halo Mass Function (RHMF). The red histogram in the upper panel shows the reference RHMF completely generated with the true halo masses. The blue histogram shows the nominal RHMF using only the mass M_o that is converted from the observable. The green histogram is the underlying RHMF yielded by the true halo mass distribution for bins that are formed by sorting the M_o . The lower panel shows the difference between the blue/green histograms and the red one.

Ranked Halo Mass Function (RHMF). It can almost be regarded as the traditional halo mass function rotated by 90 degrees, except that the halo number density is replaced by the halo mass rank, which is well defined only for a finite volume. Measurement of the RHMF is straightforward in simulation, but not so in observation, as the masses of individual halos are not accurately known. To our surprise, we find that under certain conditions (which is approximately satisfied in real cases), if the mass-ranks of halos are generated by sorting a certain type of observables instead, the resulting mean halo mass in each bin of a given mass-rank range is very close to the true one! This is true despite the fact that halos are not actually correctly ordered by their true masses in this case (due to the dispersion in the mass - observable relation). The reasons for the above phenomenon, as well as the conditions required on the observable, are given in §2. We further show that the mean halo mass in each bin can be well recovered using the stacked weak lensing signals on the background, ultimately leading to an almost unbiased estimate of the RHMF. This is shown in §3 with simulations and realistic observables. A brief conclusion and discussions are given in §4.

2. SORTING HALOS WITH OBSERVABLES

To illustrate our idea, we generate a set of halo masses using the Sheth - Tormen formula (S-T) of the Λ CDM universe (Sheth et al. 2001), with $\Omega_c = 0.223$, $\sigma_8 = 0.85$, and $\Omega_b = 0.045$. To mimic the halo mass M_o derived from an observable (through certain mass-observable relation), we add a lognormal error to the true halo mass M_t for each halo, with $\sigma_{\rm lgM} = 0.25$. In Fig.1, the red histogram in the upper panel shows the reference RHMF for the M_t , i.e., M_t is used for both ranking the halos and calculating the mean halo mass in each bin. It should be regarded as the theoretical prediction, as it is what one can easily derive from analytical formulae or N-body

simulations for any given cosmological model. It is interesting to show the blue histogram for a comparison, which uses M_o for both ranking and calculation of the mean. The result is what we call the nominal RHMF for the M_o . The blue histogram can be directly derived from observation once a mass-observable relation is given, as it completely relies on M_o . The difference between the blue and red histograms is a result of the Eddington bias. Their ratios are shown in the lower panel of Fig.1.

An interesting alternative, which is indeed the main point of this paper, is to consider plotting the mean of the true halo mass in bins that are formed by sorting M_o . The resulting RHMF is shown in the upper panel of Fig.1 with the green histogram. It is called the underlying RHMF for the M_o . Its ratio to the red histogram, i.e., the reference RHMF, is shown in the lower panel of the same figure. It is important to note that the green histogram yields almost no systematic biases in the RHMF within a large mass range. This is a very useful feature of the Λ CDM model, as we show next. We suggest that people who are not interested in this proof can directly move to the paragraph below eq.(13).

For our purpose, it is easier to work with halo masses in logarithmic units. We therefore define $\ln M_t$ as m_t , and $\ln M_o$ as m_o . For a halo of mass m_t , we define $P(m_o|m_t)dm_o$ as the probability that the observed mass is in the range of m_o and $m_o + dm_o$. Note that the observed mass here simply refers to the halo mass that is converted from an observable through a mass-observable relation. Let us also define the true halo mass function as $N_t(m_t)dm_t$, i.e., the number of halos with true masses between m_t and $m_t + dm_t$ for a given cosmic volume. Similarly, we define the number of halos with observed masses being in the range of m_o and $m_o + dm_o$ as $N_o(m_o)dm_o$. $N_o(m_o)$ and $N_t(m_t)$ have the following relation:

$$N_o(m_o) = \int_{-\infty}^{\infty} dm_t N_t(m_t) P(m_o|m_t)$$
 (1)

The mean true halo mass \overline{M}_t (not in logarithmic unit) that the observed m_o corresponds to is:

$$\overline{M}_t(m_o) = \int_{-\infty}^{\infty} dm_t \exp(m_t) P'(m_t|m_o)$$
 (2)

where $P'(m_t|m_o)$ is the probability that m_o corresponds to the true halo mass m_t . P' and P are related through:

$$P'(m_t|m_o)N_o(m_o) = P(m_o|m_t)N_t(m_t)$$
 (3)

Combining eqs.(1,2,&3), we get:

$$\overline{M}_t(m_o) = \frac{\int_{-\infty}^{\infty} dm \exp(m) P(m_o|m) N_t(m)}{\int_{-\infty}^{\infty} dm P(m_o|m) N_t(m)}$$
(4)

On the other hand, for a halo of observed mass m_o , the rank RK_o from sorting the observed mass is given by:

$$RK_o(m_o) = \int_{m_o}^{\infty} dm N_o(m)$$
 (5)

Assuming the rank RK_o in the true halo mass function corresponds to halo mass \widetilde{M}_t (not in logarithmic unit),

we have:

$$RK_o(m_o) = \int_{\ln \widetilde{M}_t}^{\infty} dm N_t(m)$$
 (6)

Eqs.(1,5,&6) lead to:

$$\int_{\ln \widetilde{M}_t}^{\infty} dm N_t(m) = \int_{m_o}^{\infty} dm \int_{-\infty}^{\infty} dm' N_t(m') P(m|m')$$
(7

Our key point is to find out whether \widetilde{M}_t , *i.e.*, the mass of the bin around the rank of RK_o for the true RHMF, can be well approximated by the \overline{M}_t from sorting an observable (the green histograms in Fig.1). For this purpose, let us assume that the true halo mass function is an exponential function: $N_t(m) \propto \exp(\alpha m)$, with α being a negative number. This form corresponds to a power law halo mass function in linear mass unit, where $\alpha-1$ is the power index. Eq.(7) then becomes:

$$-\frac{1}{\alpha}\widetilde{M}_{t}^{\alpha} = \int_{m_{o}}^{\infty} dm \int_{-\infty}^{\infty} dm' e^{\alpha m'} P(m|m') \qquad (8)$$

and eq.(4) becomes:

$$\overline{M}_t(m_o) = \frac{\int_{-\infty}^{\infty} dm P(m_o|m) e^{(1+\alpha)m}}{\int_{-\infty}^{\infty} dm P(m_o|m) e^{\alpha m}}$$
(9)

Let us further suppose that the function $P(m_o|m_t)$ can be written as $f(m_t - m_o)$, *i.e.*, the probability density function only depends on the ratio of the masses in linear units. We can then transform eq.(8) as:

$$-\frac{1}{\alpha}\widetilde{M}_{t}^{\alpha} = \int_{m_{o}}^{\infty} dm \int_{-\infty}^{\infty} dm' e^{\alpha m'} f(m' - m) \qquad (10)$$

$$= \int_{m_{o}}^{\infty} dm e^{\alpha m} \int_{-\infty}^{\infty} dm'' e^{\alpha m''} f(m'')$$

$$= -\frac{1}{\alpha} e^{\alpha m_{o}} \int_{-\infty}^{\infty} dm'' e^{\alpha m''} f(m'')$$

As a result, we get:

$$\widetilde{M}_t = e^{m_o} \left\{ \int_{-\infty}^{\infty} dm'' e^{\alpha m''} f(m'') \right\}^{\frac{1}{\alpha}}$$
 (11)

Similarly, eq.(9) can be rewritten as:

$$\overline{M}_{t}(m_{o}) = \frac{\int_{-\infty}^{\infty} dm f(m - m_{o}) e^{(1+\alpha)m}}{\int_{-\infty}^{\infty} dm f(m - m_{o}) e^{\alpha m}}$$

$$= e^{m_{o}} \cdot \frac{\int_{-\infty}^{\infty} dm' f(m') e^{(1+\alpha)m'}}{\int_{-\infty}^{\infty} dm' f(m') e^{\alpha m'}}$$
(12)

It is easy to see that when $\alpha=-1$, an interesting phenomenon emerges: $\overline{M}_t=\widetilde{M}_t$. Note that the following normalization condition is used:

$$\int_{-\infty}^{\infty} dm_o P(m_o|m_t) = 1 \tag{13}$$

which leads to $\int_{-\infty}^{\infty} dm f(m) = 1$. The above calculation provides a reason for the agreement between the green and red histograms in Fig.1. We see that the conclusion relies on two conditions:

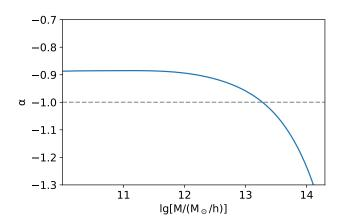


Fig. 2.— The power law index α of the halo mass function $(dn/dlnM \sim M^{\alpha})$ as a function of the halo mass in the LCDM model.

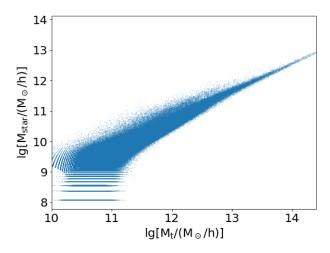


FIG. 3.— The relation between the stellar mass M_{star} and the halo mass M_t for halos from the GadgetMusic simulation of The Three Hundred project(Cui *et al.* 2018).

- 1) $N_t(m) \propto \exp(-m)$, i.e., the total halo mass within each evenly-spaced logarithmic mass bin is the same;
- 2) $P(m_o|m_t)$ is a function of $m_t m_o$ only, *i.e.*, the dispersion between the observable-inferred halo mass and the true halo mass in logarithmic units is independent of the true halo mass.

For the Λ CDM model, the value of α is indeed very close to -1 over a very wide mass range, as shown in Fig.2. The assumption that $P(m_o|m_t)$ can be written as a function of m_t-m_o is also quite commonly adopted in practice (Lima and Hu 2005; Stanek et al. 2006; Mortonson et al. 2011; Rodríguez-Puebla et al. 2013; Davidzon et al. 2017). For example, in Yang et al. (2008), it is found that the luminosity distribution for the galaxy sample has a lognormal form with a scatter nearly independent of the halo mass¹.

 1 From Fig.2, we notice that the slope $\alpha(M)$ decreases to -1.3 for $M_t \sim 10^{14.3} M_{\odot}/h$. So when a large σ_{lgM} shows up, bias would be brought to the high mass end of the RHMF. To ensure 5 percent accuracy of this method when reconstructing the RHMF, it is better to only use halos whose masses are less than $10^{14} M_{\odot}/h$

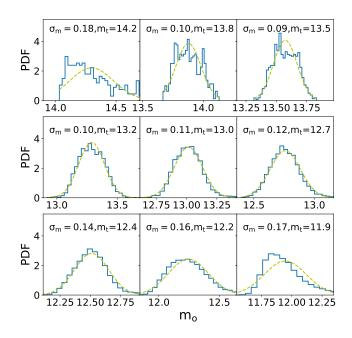


Fig. 4.— The probability distribution (PDF) of m_o (lg M_o) for a given m_t (lg M_t). The blue histogram shows the PDF of m_o converted from m_{star} shown in Fig2. The yellow line is the best-fitting gaussian function for the PDF. σ_m is the dispersion of the PDF.

However, there are also literatures assuming a varying σ_m (Saro et al. 2015; Murata et al. 2018). For instance, different from Yang et al. (2008), Zheng et al. (2007) find that the scatter of the lognormal luminosity distribution increase from 0.13 for halos with $M_t \sim 10^{13.5} M_{\odot}/h$ to 0.3 for low-mass halos with $M_t \sim 10^{11.5} M_{\odot}/h$. Therefore it is still important to check the validity of this assumption for realistic observables. As an example, in Fig.3, we plot m_{star} ($\lg M_{star}$) vs. m_t ($\lg M_t$) for halos from the GadgetMusic simulation, which is one of the zoom-in hydro-simulations from the Three Hundred project (Cui et al. 2018). By binning the halos according to their true masses, we derive the average relation between m_t and m_{star} in logarithmic space, and use the relation to convert each m_{star} into a halo mass m_o . In Fig.4, we show $P(m_o|m_t)$ for different halo masses m_t , and fit each of them with a Gaussian function. The value of σ_m is relatively stable when $m_t \gtrsim 13$, but increases gradually for smaller halo masses. Nevertheless, even in this case, we find that the underlying RHMF by sorting m_o is still quite close to the reference RHMF, as shown in Fig.5 with the green histogram (the definition of the histograms are the same as those in Fig.1). It implies that the accuracy of RHMF by sorting observables is not very sensitive to the variation of σ_m !

More generally, we carry out a series of tests to check the bias of RHMF for $d\sigma_m/dm \neq 0$ and $\alpha \neq -1$. For simplicity, we define the bias of the RHMF as the median of the relative mass biases in different bins. Since the bias also depends on the overall magnitude of σ_m , we use σ_{m13} to denote the scatter at $M_t = 10^{13} M_{\odot}/h$. In Fig.6, we show how the bias of RHMF changes with $d\sigma_m/dm$

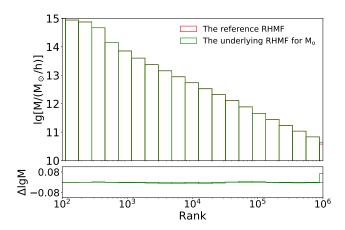


Fig. 5.— The resulting RHMF for halos from the Gadget Music simulation. The red histogram is the reference RHMF. The green histogram is the underlying RHMF for M_o .

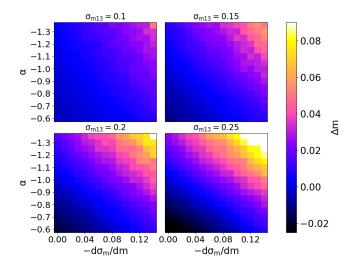


FIG. 6.— The deviation of the underlying RHMF for M_o from the reference RHMF. It is shown for different σ_{m13} , $d\sigma_m/dm$ and the power index α . For each panel, the x-axis is the $-d\sigma_m/dm$, and the y-axis is the power index α of the halo mass function. The case shown in Fig.5 corresponds to $\alpha \sim -0.9$, $-d\sigma_m/dm \sim -0.04$, and $\sigma_{m13}=0.11$.

and α for several different choices of σ_{m13} . The results indicate that the bias takes very small values ($\lesssim 0.02$) over a wide range of parameter space, demonstrating the robustness of the sorting method in constructing RHMF. In our earlier example from the GadgetMusic simulation, we have $\alpha \sim -0.9$, $d\sigma_m/dm \sim -0.04$, and $\sigma_{m13} = 0.11$, which indeed corresponds to a very small bias according to Fig.6.

3. MASS MEASUREMENT WITH WEAK LENSING

We have shown in the previous section that the RHMF can be accurately recovered by binning the observables. In this section we will show that the \overline{M}_t of each bin can be measured with weak lensing. Firstly, we will introduce the mass measurement with the lensing signals generated by the ideal Navarro-Frenk-White halos (hereafter NFW)

(Navarro *et al.* 1996). And then, we will show the mass measurement with halos in the N-body simulations.

3.1. Spherical NFW Excess Surface Density

Assuming the halos have spherical NFW profiles on average, the common way to get the halo masses is to fit the lensing signals around the halos with the NFW excess surface density (hereafter ESD) (Bartelmann 1996; Wright and Brainerd 2000).

For the spherical NFW halos, their 3D mass density are given by:

$$\rho(r) = \frac{\rho_c}{r/r_s(1 + r/r_s)^2},\tag{14}$$

where ρ_c and r_s are two parameters that describe the density profile. We parametrize the halo with the viral mass $M_{vir} = (4\pi/3)r_{vir}^3\rho_{vir}$ and the concentration $c_{vir} = r_{vir}/r_s$, where $\rho_{vir} = \Delta_{vir}\rho_{crit}$. In the ΛCDM model, the Δ_{vir} can be approximately calculated as (Bryan and Norman 1998)

$$\Delta_{vir} = 18\pi^2 + 82[\Omega_m(a) - 1] - 39[\Omega_m(a) - 1]^2.$$
 (15)

The viral radius r_{vir} is defined as the radius within which the mean mass density of the halo reach ρ_{vir} . ρ_c is given by:

$$\rho_c = \frac{\rho_{vir}}{3} \frac{c^3}{\ln(1+c) - c/(1+c)} \tag{16}$$

We define z as the distance along the line of sight, and R as the projected comoving radius from halo center, with $r = \sqrt{R^2 + z^2}$. Introducing a dimensionless quantity $x = R/r_s$, the projected surface density of the halo:

$$\Sigma(x) = \int_{-\infty}^{+\infty} \rho(r_s, x, z) dz, \tag{17}$$

and the mean surface density inside the radius R is

$$\Sigma(\langle x) = \frac{1}{\pi x^2} \int_0^x 2\pi x \Sigma(x) dx. \tag{18}$$

The ESD for the NFW halo is given by

$$\Delta\Sigma(R) = \Sigma(\langle x) - \Sigma(x) = 2\rho_c r_s f^{NFW}(x), \quad (19)$$

where the function f^{NFW} (Niikura *et al.* 2015) is given by

$$f^{NFW}(x) = \tag{20}$$

$$\begin{cases} \frac{2}{x^2} ln \frac{x}{2} + \frac{1}{1-x^2} \left(1 + \frac{2-3x^2}{x^2\sqrt{1-x^2}} cosh^{-1} \frac{1}{x} \right), (x < 1) \\ \frac{5}{3} - 2ln 2, & (x = 1) \\ \frac{2}{x} ln \frac{x}{2} - \frac{1}{x^2-1} \left(1 + \frac{2-3x^2}{x^2\sqrt{x^2-1}} cos^{-1} \frac{1}{x} \right), & (x > 1) \end{cases}$$

3.2. Measuring the RHMF with the ideal NFW halos

To test the idea of §2, we generate a set of halos according to the S-T mass function, and assign to each halo a spherical NFW density profile with concentration given by the m-c relation from Zhao et al. (2009). A mass M_o (assuming it is converted from an observable) is generated by adding a lognormal error to each M_t , with $\sigma_{1gM} = 0.25$. We rank the halos by their M_t and M_o respectively, and form the bins for measuring the

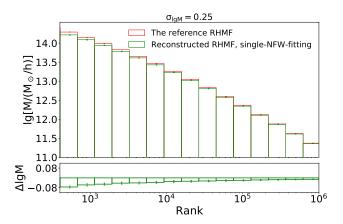


Fig. 7.— The green histogram is the reconstructed RHMF for halos sorted by M_o , with the mass of each bin recovered by fitting the stacked ESD using that of a single NFW profile. The red histogram is the reference RHMF for comparison.

RHMF. It is the purpose of this section to find out how well the underlying RHMF from the bins formed by M_o can be recovered by weak lensing, and achieve a good comparison with the results from bins formed by M_t .

If we fit the stacked profile of halos in each bin with the ESD from a single NFW profile, we find that the results from bins generated with M_t and M_o can be somewhat different, as shown in Fig.7. This is perhaps not surprising, as the ESD is not a linear function of the halo mass. The conclusion of §2 therefore cannot be extended to the case of the stacked ESD. This fact is further shown in Fig.8, in which the red and green profiles are the stacked profiles from M_t and M_o respectively. Their differences are indeed quite obvious. In other words, although the halos sorted by M_t and M_o have the same average mass in each bin, they do not share the same average ESD profile.

To avoid such a bias, we introduce the stacked-NFWfitting to take into account the distribution of the true halo masses within each bin defined by M_o . The idea is to fit the stacked ESD from observation with the stacked model ESDs for halo masses generated by a certain mass distribution. The best fitting case determines the parameters of the mass distribution, which in turn yields the arithmetic mean of the halo mass for the bin. The form of the mass distribution can in principle be worked out given the statistical relation between M_o and M_t . However, to a good approximation, we find it convenient to assume that the true halo mass within each bin simply follows a lognormal distribution. The central value and the dispersion of the distribution are the only two parameters for the fitting. As an example, in Fig.9, we show the mass distribution of m_t for a bin defined by $13.44 < m_o < 13.64$ (in blue). It is well approximated by a lognormal distribution shown as the yellow curve in the figure. The resulting RHMF is shown in Fig.10. As presented in the upper panel of the figure, the measured underlying RHMF with M_o is consistent with the reference RHMF. The residuals are found to be small as shown in the lower panel.

In summary, the underlying mean masses \overline{M}_t for bins sorted by M_o can be better measured with the stacked-

 $\sigma_{\text{IgM}} = 0.25$

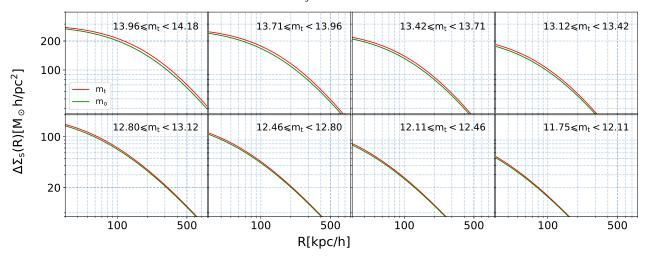


Fig. 8.— Comparison of the stacked ESD profiles for bins that are sorted by M_t (in red) and M_o (in green) respectively.

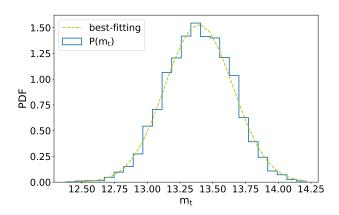


FIG. 9.— The distribution of m_t (lgM_t) for a bin formed by $13.44 < m_o < 13.64$. The blue histogram shows the actual mass distribution $P(m_t)$. It is well approximated by a lognormal distribution shown as the yellow curve.

NFW-fitting method. Fitting with the ESD of a single NFW can cause systematic biases due to the nonlinear relation between the halo mass and the ESD. In the next section, we turn to halos in N-body simulations to further check the accuracy in the recovery of RHMF, and identify problems.

3.3. Measuring the RHMF with N-body simulations

Our N-body simulation (Jing et al. 2007) assumes the Λ CDM cosmology, with $\Omega_c=0.268$, $\Omega_b=0.045$, $\Omega_{\Lambda}=0.732$, $\sigma_8=0.85$, h=0.71, and $n_s=1$. The simulation uses 1024^3 particles in a box of size $300 \mathrm{M} pc/h$, with the particle mass equal to $0.187 \times 10^{10} \mathrm{M}_{\odot}/\mathrm{h}$. Halos are identified using the standard FoF algorithm with linking length equal to 0.2. The subhalos are identified with the HBT algorithm(Han et al. 2012). The most bound particle of the central subhalo are chosen to be the halo's central position, in order to avoid the center offset effect. Considering the simulation resolution, only the FoF halos with particle number NP>100 are used. We use the mass M_{fof} from the Friends-of-Friends

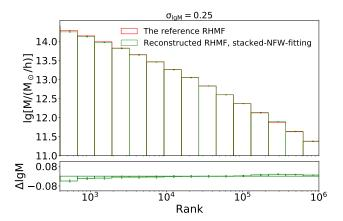


Fig. 10.— The measured RHMF with the stacked-NFW-fitting for the ideal NFW halos. The red histogram is the reference RHMF, and the green histogram shows the reconstructed RHMF for $M_{\rm e}$.

method to denote the halo mass M_t . The mass M_o from observable is generated by adding a lognormal error to M_t with $\sigma_{lqM} = 0.25$.

For our purpose, it is useful to first study the profile of the stacked ESD for the dark matter halos (Yang et al. 2006). This is done by projecting the positions of the dark matter particles of halos onto a plane perpendicular to the line of sight. Fig11 shows the stacked ESD for halos with masses M_t in a narrow mass bin ($\Delta m \sim 0.15 \text{ dex}$) around $10^{13.06} M_{\odot}/h$. The red curve is achieved with all the particles within the slice of projection ². The green curve is calculated from the particles belonging to the FoF groups of halos. Note that only when the projected distance to the halo center exceeds the viral radius (R_{vir}) , the two curves begin to deviate from each other, indicating that within R_{vir} , it is safe to fit the ESD without considering the 2-halo term.

The blue dashed curve in Fig11 shows the best-fit ESD

 $^{^2~}$ The ESD converges well for the width of the slice being larger than 10Mpc/h.

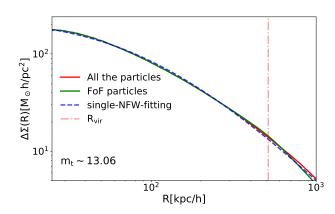


Fig. 11.— The stacked ESD for halos with masses $m_t (lg[M_t/(M_{\odot}/h)])$ in a narrow mass bin. The masses for these halos are around 13.06, and the mass bin size is about 0.15 dex. The red solid line shows the ESD achieved with all the particles within the slice of projection. The green solid line shows the ESD achieved with the particles belonging to these FoF halos. These two solid lines begin to separates only when the projected radius is larger than R_{vir} . The blue dashed line is the best-fit ESD of the NFW profile.

from a single NFW profile. We are aware that there are some scale-dependent residuals in the fitting. With the stacked-NFW-fitting method introduced in $\S 3.2$, we find that if only using the average ESD curves between $[23~{\rm kpc/h},~0.5~R_{vir}]$, the reference RHMF could be well recovered. However, we find that this mass measurement is influenced by the fitting range, for which the detailed discussion is given in appendix A.

The quality of stacked-NFW-fitting is limited by the accuracy of the NFW profile. One may consider other empirical models for describing the halo density profiles, such as gNFW(Zhao 1996; Jing and Suto 2000), Einasto(Einasto 1965), BMO(Baltz et al. 2009), Prugniel-Simien (Prugniel and Simien 1997; Merritt et al. 2006), etc.. This is however not necessary. Instead, we choose to create the model ESD directly from the N-body simulation. The method "stacked-NFW-fitting" should therefore be more generally called "stacked-model-fitting". We use halos from another independent N-body simulation to produce the ESD model as a function of the halo mass. The new ESD models can in principle be made more isotropic by averaging them over several different line-of-sight directions. However, we find that even this is not really necessary in the stacked-fitting, as stacking itself removes a significant amount of anisotropy in the final ESD model.

Similar to what is done in stacked-NFW-fitting, we assume that the true halo mass distribution in each bin ordered by M_o follows a lognormal distribution. The mean and dispersion of the distribution are achieved by fitting the stacked ESD with those stacked by the ESD models. The RHMF measured in this way is shown as the green histogram in Fig.12. It agrees very well with the reference RHMF (shown in red).

4. CONCLUSION AND DISCUSSIONS

Accurate measurement of the halo mass function is an important subject in precision cosmology. A main concern in this field is about building up the relation between

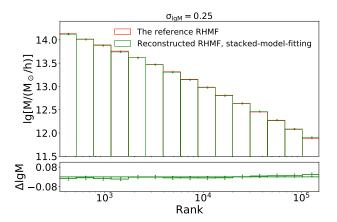


FIG. 12.— The green histogram shows the RHMF measured with the stacked ESD model created from the N-body simulation for bins formed by M_o . The red histogram is the reference RHMF.

the obervable and the underlying halo mass. The dispersion between the observable and the halo mass is also required to be known well to overcome the Eddington bias in traditional methods. In this paper, we point out a new way of measuring the halo mass function that does not require accurate knowledge of the mass-observable relation. In the new method, the observable is used only for the purpose of sorting the halos as if the observable were the true halo mass. It is to our surprise that the resulting mean halo mass of each bin is indeed very close to its counterpart from sorting the true halo mass! In §2, we have shown that this phenomenon relies on two conditions: 1. the halo mass function is close to a powerlaw form with a power index close to -2, *i.e.*, the total halo mass within each unitary logarithmic scale is approximately a constant (This condition is approximately satisfied by the Λ CDM models over a large mass range); 2. statistically, the observable has a monotonous relation with the halo mass, and the dispersion of the relation changes slowly with the halo mass.

Making use of this appealing feature, we show how to use weak lensing to accurately recover the so-called Ranked Halo Mass Function (RHMF), *i.e.*, the halo mass as a function of the mass order/rank within a certain cosmic volume. This can be done by modeling the true halo mass distribution as a lognormal function in each bin defined by the observable, and fitting their stacked excess surface density profile (ESD) with stacked ESD models from either NFW or N-body simulations directly. In this way, halo mass function from the cosmological simulation can be directly compared with that from observations without careful modelling of the mass-observable relation!

We point out that although the study in this work uses the Friends-of-Friends mass to define the halo mass, other mass definitions such as M_{vir} , M_{200} , and M_{500} are equally good as long as the same mass definition is used for both constructing the reference RHMF and creating the ESD models, because these definitions have very tight relations with each other. Note that changing the mass definition leads to a change in the halo mass function and the reference RHMF, meanwhile the constructed RHMF from the observables changes correspondingly. The mass

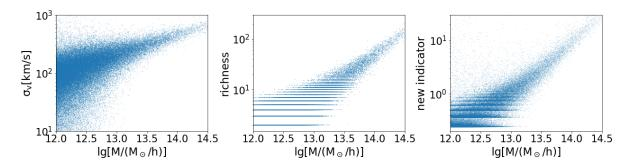


Fig. 13.— The halo mass vs. observables for the N-body simulation. The left panel shows halo mass vs. line-of-sight velocity dispersion (σ_v) . The middle panel shows the halo mass vs. richness (r). The right panel shows the halo mass vs. the form of $r/r_0 + 2\sigma_v^4/\sigma_{v0}^4$, with r_0 and σ_{v0} being constants.

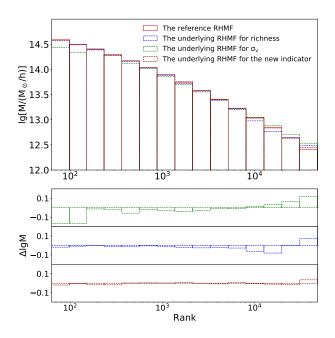


Fig. 14.— The resulting RHMF for the observable. The red solid histogram is the reference RHMF. The blue and green dashed histogram show the underlying RHMFs for richness and σ_v respectively. The marroon dashed histogram show the underlying RHMF for the mass indicator defined as a function of σ_v and richness.

definition therefore does not affect the comparison of the RHMF's from observation and simulation. We consider this feature a significant advantage of our method. In fact, this is in line with the main idea of this paper. If we regard the different mass definitions as different observables, they shall share the same underlying RHMF as long as the dispersions of their mutual relations are moderate. It can be viewed as an option to achieve precise cosmological constraints without worrying too much about the robustness of the halo mass definition.

For accurate reconstruction of the RHMF, it is better to have an observable (used as the mass estimator) that has a tight relation (less scatter) with the halo mass. For this purpose, one can consider building an observable as a function of the existing/familiar ones. For instance, the subhalo velocity dispersion σ_v along the line of sight is found to have large scatters with the halo mass M_t , as shown in the left panel of Fig.13, in which many small halos are found to have great σ_v . The situation for rich $ness^3 r$ is somewhat similar, as shown in the middle panel of Fig.13. As an improvement, we consider the combination of these two quantities in the form of $r/r_0 + 2\sigma_v^4/\sigma_{v0}^4$, which seems to have more tight relations with M_t , as shown in the right panel of Fig.13. Here, the r_0 is set to be the value of richness at $m_t = 13$ using the average relationship between the richness and the halo mass. σ_{v0} is similarly defined, but with $m_t = 13.5$. Its underlying RHMF becomes more consistent with the reference RHMF with this new mass indicator, as shown in Fig.14.

In construction the RHMF, there are issues that have not been discussed in this work. For example, the off-centering effect in the stacking of the background lensing signals, subhalo contribution of the satellite galaxies, stellar contribution of the central galaxies (see e.g. Luo et al. 2018, for more details), as well as the baryonic effect on the halo density profile, the miss-identification of clusters/groups in galaxy redshift surveys (Yang et al. 2007). In our future work, we plan to address these issues when applying this method on the real data.

ACKNOWLEDGMENTS

We thank Yipeng Jing for providing us the N-body simulations. We also thank Weiguang Cui for providing us the halo catalogue of The Three Hundred simulation. This work is supported by the National Key Basic Research and Development Program of China (No.2018YFA0404504), the National Key Basic Research Program of China (2015CB857001, 2015CB857002), the NSFC grants (11673016, 11433001, 11621303). JJZ is supported by China Postdoctoral Science Foundation 2018M632097.

REFERENCES

 $^{^{3}}$ We define the halo richness as the number of its subhalos with

C. Lacey and S. Cole, MNRAS 262, 627 (1993).

- W. H. Press and P. Schechter, ApJ 193, 437 (1974).
 S. D. M. White, G. Efstathiou, and C. S. Frenk, MNRAS 262, 1023 (1993).
- A. Vale and J. P. Ostriker, MNRAS 353, 189 (2004), astro-ph/0402500.
- astro-ph/0402500.
 E. S. Sheldon, D. E. Johnston, R. Scranton, B. P. Koester, T. A. McKay, H. Oyaizu, C. Cunha, M. Lima, H. Lin, J. A. Frieman, R. H. Wechsler, J. Annis, R. Mandelbaum, N. A. Bahcall, and M. Fukugita, ApJ 703, 2217 (2009), arXiv:0709.1153.
 A. H. Bauer, C. Baltay, N. Ellman, J. Jerke, D. Rabinowitz, and R. Scalzo, ApJ 749, 56 (2012), arXiv:1202.1371.
 R. Mandelbaum, U. Seljak, and C. M. Hirata, J. Cosmology Astropart. Phys. 8, 006 (2008), arXiv:0805.2552.
 G. W. Pratt, J. H. Croston, M. Arnaud, and H. Böhringer, A&A 498, 361 (2009), arXiv:0809.3784.
 M. Bartelmann and P. Schneider, Phys. Rep. 340, 201 (2001)

- M. Bartelmann and P. Schneider, Phys. Rep. 340, 291 (2001), astro-ph/9912508.
- P. Schneider, arXiv Astrophysics e-prints (2005), astro-ph/0509252
- R. A. Sunyaev and Y. B. Zeldovich, Comments on Astrophysics and Space Physics 4, 173 (1972).

 A. Biviano, G. Murante, S. Borgani, A. Diaferio, K. Dolag, and
- M. Girardi, A&A 456, 23 (2006), astro-ph/0605151.
 E. Munari, A. Biviano, S. Borgani, G. Murante, and D. Fabjan, MNRAS 430, 2638 (2013), arXiv:1301.1682 [astro-ph.CO].
- M. Lima and W. Hu, Phys. Rev. D 72, 043006 (2005), astro-ph/0503363.
- Y. P. Jing, H. J. Mo, and G. Börner, ApJ 494, 1 (1998), astro-ph/9707106.
- A. A. Berlind and D. H. Weinberg, ApJ 575, 587 (2002), astro-ph/0109001.

- astro-ph/0109001.

 X. Yang, H. J. Mo, and F. C. van den Bosch, MNRAS 339, 1057 (2003), astro-ph/0207019.

 Z. Zheng, A. A. Berlind, D. H. Weinberg, A. J. Benson, C. M. Baugh, S. Cole, R. Davé, C. S. Frenk, N. Katz, and C. G. Lacey, ApJ 633, 791 (2005), astro-ph/0408564.

 F. C. van den Bosch, X. Yang, H. J. Mo, S. M. Weinmann, A. V. Macciò, S. More, M. Cacciato, R. Skibba, and X. Kang, MNRAS 376, 841 (2007), astro-ph/0610686.

 I. Zehavi et al., ApJ 736, 59 (2011), arXiv:1005.2413.

 A. Leauthaud, J. Tinker, P. S. Behroozi, M. T. Busha, and R. H. Wechsler, ApJ 738, 45 (2011), arXiv:1103.2077.

 X. Yang, H. J. Mo, F. C. van den Bosch, Y. Zhang, and J. Han, ApJ 752, 41 (2012), arXiv:1110.1420.

 A. Rodríguez-Puebla, V. Avila-Reese, X. Yang, S. Foucaud, N. Drory, and Y. P. Jing, ApJ 799, 130 (2015), arXiv:1408.5407.

 Y. Zu and R. Mandelbaum, MNRAS 457, 4360 (2016),

- Y. Zu and R. Mandelbaum, MNRAS 457, 4360 (2016), arXiv:1509.06758
- arXiv:1509.06758.

 H. Guo, Z. Zheng, P. S. Behroozi, I. Zehavi, C.-H. Chuang,
 J. Comparat, G. Favole, S. Gottloeber, A. Klypin, F. Prada,
 S. A. Rodríguez-Torres, D. H. Weinberg, and G. Yepes,
 MNRAS 459, 3040 (2016), arXiv:1508.07012.

 A. Rodríguez-Puebla, J. R. Primack, V. Avila-Reese, and S. M.
 Faber, MNRAS 470, 651 (2017), arXiv:1703.04542.
- H. Guo, X. Yang, and Y. Lu, ApJ 858, 30 (2018), arXiv:1804.01993.
- D. Obreschkow, S. G. Murray, A. S. G. Robotham, and T. Westmeier, MNRAS **474**, 5500 (2018), arXiv:1712.00149.
- A. S. Eddington, MNRAS 474, 5300 (2018), arXiv:1712.00149.
 A. S. Eddington, MNRAS 73, 359 (1913).
 A. Leauthaud, S. Saito, S. Hilbert, A. Barreira, S. More,
 M. White, S. Alam, P. Behroozi, K. Bundy, J. Coupon,
 T. Erben, C. Heymans, H. Hildebrandt, R. Mandelbaum,
 L. Miller, B. Moraes, M. E. S. Pereira, S. A. Rodríguez-Torres,
 F. Schmidt, H.-Y. Shan, M. Viel, and F. Villaescusa-Navarro,
 MNRAS 467, 2024 (2017) avyintell.08606

MNRAS 467, 3024 (2017), arXiv:1611.08606.

M. Simet, T. McClintock, R. Mandelbaum, E. Rozo, E. Rykoff, E. Sheldon, and R. H. Wechsler, MNRAS 466, 3103 (2017), arXiv:1603.06953.

- R. Murata, T. Nishimichi, M. Takada, H. Miyatake, M. Shirasaki, S. More, R. Takahashi, and K. Osato, ApJ 854, 120 (2018), arXiv:1707.01907.
- R. K. Sheth, H. J. Mo, and G. Tormen, MNRAS 323, 1 (2001), astro-ph/9907024.

Appendices

A. THE MASS MEASUREMENT FOR HALOS FROM THE N-BODY SIMULATION WITH THE NFW MODEL

- R. Stanek, A. E. Evrard, H. Böhringer, P. Schuecker, and B. Nord, ApJ 648, 956 (2006), astro-ph/0602324.
 M. J. Mortonson, W. Hu, and D. Huterer, Phys. Rev. D 83, 023015 (2011), arXiv:1011.0004 [astro-ph.CO].
 A. Rodríguez-Puebla, V. Avila-Reese, and N. Drory, ApJ 767, 92 (2013), arXiv:1302.0005.

- U23015 (2011), arXiv:1011.0004 [astro-ph.CO].
 A. Rodríguez-Puebla, V. Avila-Reese, and N. Drory, ApJ 767, 92 (2013), arXiv:1302.0005.
 I. Davidzon, O. Ilbert, C. Laigle, J. Coupon, H. J. McCracken, I. Delvecchio, D. Masters, P. Capak, B. C. Hsieh, O. Le Fèvre, L. Tresse, M. Bethermin, Y.-Y. Chang, A. L. Faisst, E. Le Floc'h, C. Steinhardt, S. Toft, H. Aussel, C. Dubois, G. Hasinger, M. Salvato, D. B. Sanders, N. Scoville, and J. D. Silverman, A&A 605, A70 (2017), arXiv:1701.02734.
 X. Yang, H. J. Mo, and F. C. van den Bosch, ApJ 676, 248 (2008), arXiv:0710.5096.
 W. Cui, A. Knebe, G. Yepes, F. Pearce, C. Power, R. Dave, A. Arth, S. Borgani, K. Dolag, P. Elahi, R. Mostoghiu, G. Murante, E. Rasia, D. Stoppacher, J. Vega-Ferrero, Y. Wang, X. Yang, A. Benson, S. A. Cora, D. J. Croton, M. Sinha, A. R. H. Stevens, C. A. Vega-Martínez, J. Arthur, A. S. Baldi, R. Cañas, G. Cialone, D. Cunnama, M. De Petris, G. Durando, S. Ettori, S. Gottlöber, S. E. Nuza, L. J. Old, S. Pilipenko, J. G. Sorce, and C. Welker, MNRAS 480, 2898 (2018), arXiv:1809.04622.
 A. Saro, S. Bocquet, E. Rozo, B. A. Benson, J. Mohr, E. S. Rykoff, M. Soares-Santos, L. Bleem, S. Dodelson, P. Melchior, F. Sobreira, V. Upadhyay, J. Weller, T. Abbott, F. B. Abdalla, S. Allam, R. Armstrong, M. Banerji, A. H. Bauer, M. Bayliss, A. Benoit-Lévy, G. M. Bernstein, E. Bertin, M. Brodwin, D. Brooks, E. Buckley-Geer, D. L. Burke, J. E. Carlstrom, R. Capasso, D. Capozzi, A. Carnero Rosell, M. Carrasco Kind, I. Chiu, R. Covarrubias, T. M. Crawford, M. Crocce, C. B. D'Andrea, L. N. da Costa, D. L. DePoy, S. Desai, T. de Haan, H. T. Diehl, J. P. Dietrich, P. Doel, C. E. Cunha, T. F. Eiffer, A. E. Evrard, A. Fausti Neto, E. Fernandez, B. Flaugher, P. Fosalba, J. Frieman, C. Gangkofher, E. Gaztanaga, D. Gerdes, D. Gruen, R. A. Gruendl, N. Gupta, C. Hennig, W. L. Holzapfele, K. Honscheid, B. Jain, D. James, K. Kuehn, N. Kuropatkin, O. Lahav, T. S. Li, H. Lin, M. A. G. Maia, M. March, J. L. Marshall, P. Martini, M. McDonal
- (1996), astro-ph/9508025
- M. Bartelmann, A&A 313, 697 (1996), astro-ph/9602053.
- C. O. Wright and T. G. Brainerd, ApJ 534, 34 (2000).
- G. L. Bryan and M. L. Norman, ApJ 495, 80 (1998), astro-ph/9710107.
- astro-pn/9710107.
 H. Niikura, M. Takada, N. Okabe, R. Martino, and R. Takahashi, PASJ **67**, 103 (2015), arXiv:1504.01413.
 D. H. Zhao, Y. P. Jing, H. J. Mo, and G. Börner, ApJ **707**, 354 (2009), arXiv:0811.0828.
- Y. P. Jing, Y. Suto, and H. J. Mo, ApJ 657, 664 (2007),
- astro-ph/0610099.

 J. Han, C. S. Frenk, V. R. Eke, L. Gao, S. D. M. White,
 A. Boyarsky, D. Malyshev, and O. Ruchayskiy, MNRAS 427,
 1651 (2012), arXiv:1207.6749 [astro-ph.CO].

 X. Yang, H. J. Mo, F. C. van den Bosch, Y. P. Jing, S. M.
- Weinmann, and M. Meneghetti, MNRAS 373, 1159 (2006),
- astro-ph/0607552 H. Zhao, MNRAS 278, 488 (1996), astro-ph/9509122
- Y. P. Jing and Y. Suto, The Astrophysical Journal 529, L69
- J. Einasto, Trudy Astrofizicheskogo Instituta Alma-Ata 5, 87 (1965).
- E. A. Baltz, P. Marshall, and M. Oguri, J. Cosmology Astropart. Phys. 1, 015 (2009), arXiv:0705.0682.
- P. Prugniel and F. Simien, A&A 321, 111 (1997).
 D. Merritt, A. W. Graham, B. Moore, J. Diemand, and
 B. Terzić, The Astronomical Journal 132, 2685 (2006).
 W. Luo, X. Yang, T. Lu, F. Shi, J. Zhang, H. J. Mo, C. Shu,
 L. Fu, M. Radovich, J. Zhang, N. Li, T. Sunayama, and
 L. Wang, ApJ 862, 4 (2018), arXiv:1712.09030.
 X. Yang, H. J. Mo, F. C. van den Bosch, A. Pasquali, C. Li, and

M. Barden, ApJ 671, 153 (2007), arXiv:0707.4640

In §3.2, for the case of ideal NFW halos, we show that the underlying mean masses for bins sorted by M_o

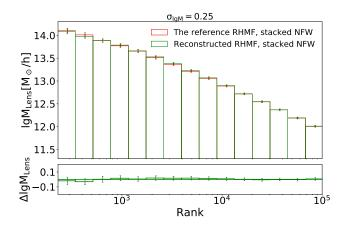


Fig. 15.— The measured RHMF with the stacked-NFW-fitting, using the stacked ESD curve between [23kpc/h, 0.5 R_{vir}]. The green histogram shows the reconstructed RHMF for M_o . The red histogram is the reference RHMF.

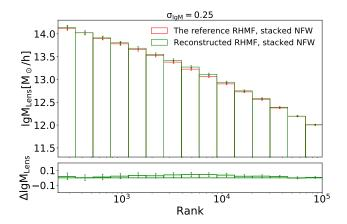


Fig. 16.— The measured RHMF with the stacked-NFW-fitting, using the stacked ESD curve between [23kpc/h, 0.7 R_{vir}]. The green histogram shows the reconstructed RHMF for M_o . The red histogram is the reference RHMF.

can be better measured with the stacked-NFW-fitting method. In this section, for halos from the N-body

simulation, we perform the mass measurement in a similar way. The only difference is that we introduce an additional parameter c_{ratio} in the fitting to account for a mass-independent multiplicative deviation of the concentration from the m-c relation of Zhao *et al.* (2009).

With the stacked-NFW-fitting, we find that if only using the stacked ESD curves between $[23\mathrm{kpc/h}, 0.5~R_{vir}]$, the reference RHMF could be well recovered, as shown in Fig.15. When attempting to extend the fitting range to, say, $0.7~R_{vir}$, we find that the noticeable inconsistencies show up between the measured RHMF and the reference RHMF, as shown in Fig.16. In fact, varying the inner fitting range would also influence the fitting results. Considering the scale-dependent residuals between the best fitted NFW ESD and the stacked ESD in Fig11, this phenomenon is not surprising.

During the fitting, to estimate the viral radius R_{vir} for the M_o formed mass bin, we would firstly repeat the single-NFW-fitting for several times. For each time, we fit the stacked ESD curve over a radius less than R_{max} . For the first time, R_{max} is set to be 5 Mpc/h. After achieving the best fitted mass M_{vir} , we update the value of R_{max} with the corresponding R_{vir} . After loop this operation for a few times, the value of R_{vir} becomes stable.

In the above, we recover the underlying mean mass for the M_o formed ranking bin with the stacked-NFWfitting. However, the underlying mass recovered in this way differs from the \overline{M}_t , in which M_t is set according to M_{fof} . So to make a more fair comparison, we choose to generate the reference RHMF also through fitting the stacked ESD profile, by modeling the halo mass distribution for the M_t formed ranking bin. The resulting RHMF is shown as the red histogram in Fig.15 and Fig.16. We point out that for other kind of mass definitions, such as M_{200} , M_{vir} etc., almost the same stacked ESDs are got for the same ranking bin. Actually, we find that as long as the dispersion between these mass definitions are less than 0.15 dex, the shape and amplitude of their stacked ESD would be almost unchanged. Since these mass definitions are tight related, the comparison between the reference RHMF and the reconstructed RHMF would not be affected by the choice of M_t .